

Communication

# Dielectrophoresis-Based Biosensor for Detection of the Cancer Biomarkers CEA and CA 242 in Serum

Fleming Dackson Gudagunti , Srilakshmi G. Gundlakunta and Ivan T. Lima, Jr. \* 

Department of Electrical and Computer Engineering, North Dakota State University, Fargo, ND 58108-6050, USA; fleming.gudagunti@ndsu.edu (F.D.G.); s.gundlakunta@ndsu.edu (S.G.G.)

\* Correspondence: ivan.lima@ndsu.edu

**Abstract:** We show that dielectrophoresis (DEP) spectroscopy is an effective transduction mechanism for detection of the concentration levels of the pancreatic cancer biomarkers cancer antigen (CA) 242 and carcinoembryonic antigen (CEA) in serum. We noticed a frequency dependence of the negative DEP force applied by interdigitated electrodes on functionalized polystyrene microspheres (PM) with respect to changes in the number of these cancer antigens bound to the PM. An electrode array with a well-defined gradient of the electric field was designed and used, which enabled the automation of the signal processing and reproducibility of the signal acquired by the biosensor.

**Keywords:** dielectrophoresis; image processing; pancreatic cancer biomarkers



**Citation:** Gudagunti, F.D.; Gundlakunta, S.G.; Lima, I.T., Jr. Dielectrophoresis-Based Biosensor for Detection of the Cancer Biomarkers CEA and CA 242 in Serum. *Chemosensors* **2022**, *10*, 104. <https://doi.org/10.3390/chemosensors10030104>

Academic Editor: Larisa Lvova

Received: 18 January 2022

Accepted: 7 March 2022

Published: 10 March 2022

**Publisher's Note:** MDPI stays neutral with regard to jurisdictional claims in published maps and institutional affiliations.



**Copyright:** © 2022 by the authors. Licensee MDPI, Basel, Switzerland. This article is an open access article distributed under the terms and conditions of the Creative Commons Attribution (CC BY) license (<https://creativecommons.org/licenses/by/4.0/>).

## 1. Introduction

Pancreatic cancer accounts for about 3% of all cancers and about 7% of all cancer deaths [1], which makes it the fourth leading cause of death due to cancer. The average five-year survival rate for pancreatic cancer patients after the diagnosis is lower than 6% [2,3]. Even though different types of tumors can develop in the pancreas, a specific histologic subtype named pancreatic ductal adenocarcinoma is the most common type of pancreatic tumor. One of the biggest reasons for this tumor causing such a high mortality rate is the lack of prescreening methods and early detection techniques. Although the cure for this disease is still not available on the market, surgery offers a realistic chance for survival but often does not lead to a cure. Even if all detectable cancer tumors are removed, often a few cancer cells have already spread to other parts of the body. These cells can metastasize into new tumors over time, which become more difficult to treat [4,5].

Biomarkers are key in detecting any form of cancer as they can distinguish between benign and malignant cells and hence differentiate among the tumor types [6,7]. Some of the prognostic biomarkers include nucleic acids [8,9], proteins, small molecules, exosomes, antibodies, and metabolites that are consistently used for diagnosis, treatment, and therapies [10–19]. For diagnostic accuracy, a single biomarker does not yield good specificity and sensitivity. Thus, we need to have a combination of biomarkers to increase the specificity and the sensitivity of the diagnostic accuracy [15].

Some of the popular pancreatic cancer protein biomarkers are CA 19-9, HE4, AGR2, MMP-7, IGFBP2/3, haptoglobin, CA 494, CA 242, CEA, carboxypeptidase A, thrombospondin –2 NGAL, TPS, Osteoprotegerin, macrophage inhibitory cytokine, TIMP-1, MMP-9, MUC4, MUC1, and CAM1 [16–25]. Among these biomarkers, only CA 19-9 is an FDA-approved biomarker. Elevated levels of CA 19-9 above 37 U/mL have been associated with pancreatic cancer. However, the detection of CA 19-9 has demonstrated modest effectiveness for the prognosis of pancreatic cancer.

In addition to CA 19-9, CA 242 is a potential complementing biomarker of pancreatic cancer in the early stages. The epitope of CA 242 is an acid-containing carbohydrate structure that is found in the form of glycoproteins or glycolipids on the cell surface. The patients with pancreatic cancer in the early stage showed signs of increased levels of CA 242.

CA 242 has slightly smaller sensitivity and specificity compared to CA 19-9 in the diagnosis of pancreatic cancer [26–29]. Zhang et al. [30] showed that the simultaneous detection of CA 19-9 and CA 242 enables the highest sensitivity in the detection of pancreatic cancer when compared with the detection of CA 19-9 alone or when it is combined with the detection of other cancer biomarkers. CEA is another widely used cancer biomarker that has been extensively used in clinical practice. Patients with cancers such as gastrointestinal cancer, pancreatic cancers, lung carcinoma, breast carcinoma, and ovarian carcinoma have increased levels of CEA [31–36]. Chemiluminescence immunoassay (CLIA) and enzyme-linked immunosorbent immunoassay (ELISA) have been generally used in the detection of CEA and CA 242. Some of the limitations of these techniques include the large sample volume requirement, high cost, and complexity [20].

In a previous study [20], we investigated the effectiveness of a DEP-based biosensor for CA 19-9 in a phosphate-buffered saline (PBS) solution using an electrode array that did not have a clearly defined field distribution, since it was designed for metal-enhanced fluorescence studies. Moreover, biosensor assays in PBS do not demonstrate the robustness of the method in the presence of a complex medium such as blood serum. In this paper, we extended that work in several ways. First, we investigated the effectiveness of DEP spectroscopy when applied to the detection of two additional cancer antigens: CEA and CA 242, including their respective clinically relevant detection thresholds. Second, we investigated the effectiveness of that biosensor for the detection of those cancer antigens in Bovine Albumin serum (BSA) to demonstrate that the transduction mechanism of this biosensor is effective even in the presence of a complex biological medium. Third, we carried out this study using a new electrode array that we designed with a well-defined gradient of the electric field that is suitable for automation and repeatability even when different electrodes in the array or different electrode arrays are used. We think that the combination of these improvements demonstrates that DEP-based biosensors have good potential for use in clinical practice using samples from patients.

## 2. Materials and Methods

### 2.1. Interdigitated Microelectrode Array

The direction of movement for the dielectric particle due to DEP depends upon the relative polarizability of the particle and the medium and on the presence of a large gradient of the electric field intensity produced by electrodes. The polarizability of the particle is determined by the Clausius-Mossotti factor, which depends on the complex permittivity of the medium and of the particle [37,38]. In this experiment, we used an interdigitated electrode array that were designed and fabricated at North Dakota State University. Unlike the electrode array that we used in a previous study on CA 19-9 detection that we carried out [20], this electrode array produces a well-defined gradient of the electric field that enables the automation of the signal acquisition and repeatability of the results across different electrode arrays. Microscopic images of the electrode array are shown in Figure 1.

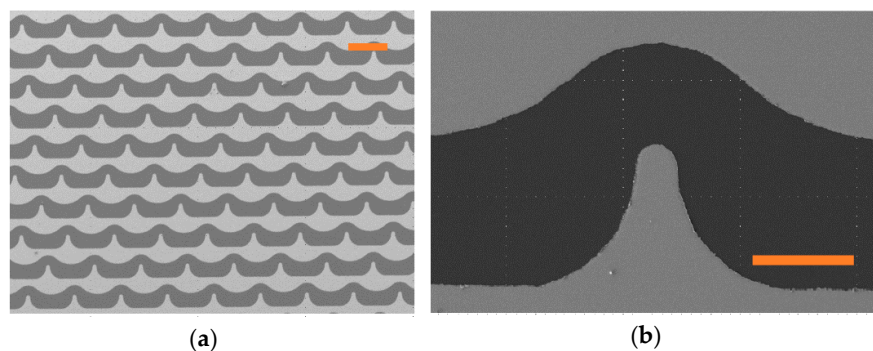


**Figure 1.** Interdigitated electrodes were used in the experiments. (a) Microelectrode array image obtained with a 10× objective with an orange scale bar that indicates 200 μm. (b) Microelectrode array image obtained with a 40× objective with an orange scale bar that indicates 50 μm.

## 2.2. Sample Preparation of CEA

**Step 1: Streptavidin binding to biotinylated PM.** Biotinylated PM with 740 nm diameters were purchased from Spherotech Inc. The first step in the preparation of the samples consisted of binding the biotinylated PM with the antigen Streptavidin purchased from Vector Labs Inc. Biotin acts as a conjugate to the protein Streptavidin and forms a strong bond with very high affinity. This process is carried out by first adding a 3  $\mu\text{L}$  Streptavidin solution to a 10  $\mu\text{L}$  biotinylated PM solution in a centrifuge tube to have 100% binding, according to the manufacturer's recommendation. The total volume was set to 400  $\mu\text{L}$  by adding  $0.01\times$  PBS solution. Then, the sample was uniformly mixed using a vortex machine and left on a shaker for 20 min for the Streptavidin–biotin-binding process. After 20 min, the tube was centrifuged at 5000 rpm for 14 min to remove the unbound Streptavidin molecules and the buffer.

**Step 2: Biotinylated CEA antibody binding to the biotinylated PM + Streptavidin.** Each Streptavidin molecule can bind up to four biotin molecules. One binding site of each Streptavidin molecule was used to bind that Streptavidin molecule with the PM. The remaining three Streptavidin binding sites were bound with the three biotinylated CEA antibodies. First, 3  $\mu\text{L}$  of the biotinylated CEA antibody was added into 397  $\mu\text{L}$  of  $0.01\times$  PBS to have 100% binding of the biotinylated antibodies with all the Streptavidin molecule binding sites, according to the manufacturer's requirement. Then, this sample was added to the solution with Streptavidin–biotin PM and uniformly mixed using a vortex machine. After that, the sample was kept on a shaker for 20 min for the biotinylated CEA antibodies to bind with the Streptavidin molecules of the PM. After 20 min, the tube was centrifuged at 5000 rpm for 14 min to remove the buffer. This completed the preparation of the antibody-functionalized PM for the assay.

**Step 3: CEA antigen binding to the PM + Streptavidin + CEA antibody.** For this process, different concentrations of the CEA antigen, including 0 ng/mL, 5 ng/mL, 10 ng/mL, and 20 ng/mL, were prepared in a total volume of 400  $\mu\text{L}$   $0.1\times$  BSA buffer. Then, this sample was added to the CEA antibody-bound PM and mixed uniformly using a vortex machine. After that, the sample was kept on a shaker for 30 min. In this procedure, BSA emulates a complex biological fluid. The sample was centrifuged at 5000 rpm for 14 min to remove the medium used in the assay. Finally, 200  $\mu\text{L}$  of  $0.01\times$  PBS buffer was added to the centrifuge tube and mixed uniformly. This last procedure ensured that the solution in which the DEP experiments would be conducted had a fixed conductivity. This procedure will be essential in clinical assays since blood serum from different individuals or the same individual on different days can have different conductivities. A schematic representation of these experimental procedures is shown in Figure 2.

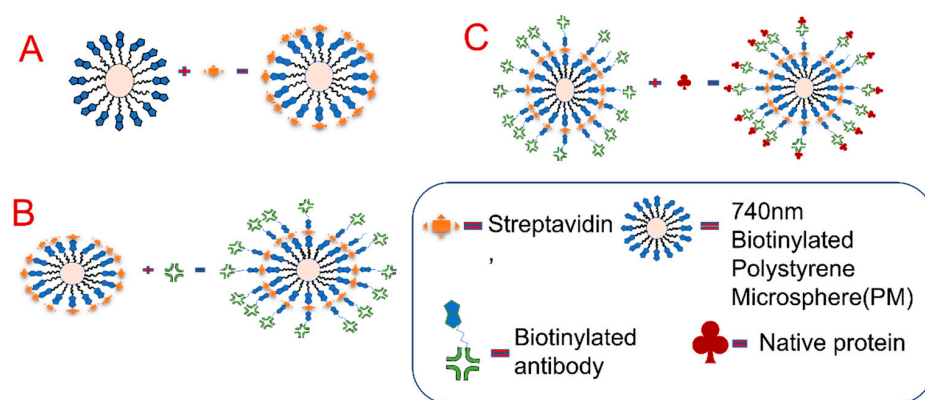


**Figure 2.** Schematic representation of the sample preparation (Biotinylated polystyrene microspheres (PM) + Streptavidin + Biotinylated CA 242/CEA Monoclonal Antibody) with the antigen Native Protein CA 242/CEA, assuming binding in all of the available sites of the antibody. (A) Binding of biotinylated PM with streptavidin. (B) Functionalization of the PM with antibodies. (C) Assay for the detection of the antigens.

Using information from the manufacturer of the biotinylated PM, Streptavidin, the antigens, and the antibodies, there are a total of  $5.78 \times 10^4$  antibody binding sites for the antigens on each PM. Since there are a total of  $3.55 \times 10^7$  PM in the sample and  $3.13 \times 10^{10}$  molecules of CEA with the concentration of 10 ng/mL of CEA in 400  $\mu$ L  $0.1 \times$  BSA buffer, 0.51% of the antibody binding sites were bound to CEA molecules in that assay.

### 2.3. Sample Preparation of CA 242

The preparation of the assay for the detection of CA 242 is similar to the preparation of the assay for the detection of CEA. After Streptavidin molecules bind to biotinylated PM, biotinylated CA 242 antibodies bind to the Streptavidin molecules. For this study, we spiked different concentration levels of CA 242 in  $0.1 \times$  BSA. Since 20 U/mL is the cutoff level for the early detection of CA 242, we prepared assays with the concentration levels of CA 242 at 0 U/mL, 10 U/mL, 20 U/mL, and 40 U/mL. The assay with 0 U/mL was a control sample without the native antigen of CA 242 attached to the PM functionalized with CA 242 antibodies.

## 3. Results

To measure the drift velocity for a particular frequency, positive DEP needs to be applied, wherein the PM is attracted to the edge of the convex electrodes, followed by negative DEP, which causes the PM to be repelled from the edge of the convex electrode. With the onset of the experiment, the software set a range of frequencies to sweep through, with the lowest frequency being 0.5 MHz and the highest frequency set at 2 MHz in steps of 0.3 MHz. The peak-to-peak voltage was set to 10 V. The time intervals set for the positive and negative DEP were 120 ms and 80 ms respectively. These time intervals were determined from our previous study [20]. The cycle was repeated for a series of frequency ranges until hitting the final set point. The drift velocity of the PM functionalized with antibody to CEA/CA 242 as a function of the frequency of the electric field due to DEP was measured using an application that we developed using Microsoft Foundation Classes in C++.

We validated this biosensor technique for the detection of CEA and CA 242 by carrying out experiments using our automated real-time image processing software for image processing and analysis. The sample was pipetted onto the microelectrodes, and the microscope was focused on the electrode's region of interest. Using a TDS/Conductivity/Salinity Pen from BME Lab and Science, we measured the conductivity of  $0.01 \times$  PBS at 0.05 S/m. Once the software was started, the frequency sweep was initiated for the DEP spectrum measurement. The functionalized PMs experienced an attractive force towards the edge of the electrodes at 10 kHz with 10 V peak-to-peak using the function generator, as shown in Figure 3. This frequency produced a positive DEP. The function generator maintained this frequency and voltage for 60 s, which concentrated the PM on the convex edge of the electrodes. At the end of that period, the frequency was switched to 0.5 MHz with 10 V peak-to-peak for 80 ms. This produced a negative DEP; hence, the functionalized PMs experienced a repulsive force that moved the PM away from the convex edge of the electrode. The drift velocity of the PMs was proportional to the DEP force. As the software is capable of capturing images at 25 frames per second from the live video feed, the movement of the functionalized PMs was tracked along the axis of the electrode within the region of interest. We calculated the drift velocity of the functionalized PMs after obtaining the center of mass of the PMs at the onset of negative DEP, which was produced with the frequency 0.5 MHz and 80 ms later. This was repeated for additional frequencies ranging from 0.8 MHz to 2 MHz, in which the PM also experienced a negative DEP force. The elliptical region shown with orange arrows in Figure 3b was integrated to produce a one-dimensional histogram from which the center of mass of the PM was calculated in each of the two images. The drift velocity was calculated by dividing the difference between the centers of mass by the time elapsed between the acquisition of these two images.

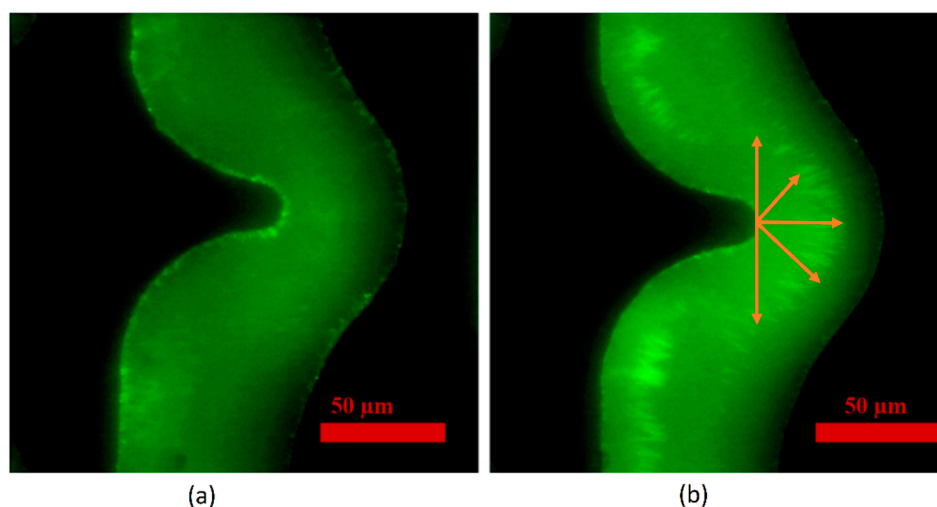


**Figure 3.** Images used in the calculation of the drift velocity due to negative DEP. (a) A single interdigitated electrode pair 60 s after the application of 10 kHz, which produced positive DEP. (b) The same electrode pair 80 ms after the application of 500 kHz, which produced negative DEP. The concentration of CA 242 in this solution is 20 U/mL. The interdigitated electrode pair is visible as a darker region in the picture. The bright layer visible on the edge of the electrode was formed by the accumulation of the sample. As the frequency was changed to induce negative DEP, the antigen-bound PM was repelled from the electrode. The scale bar in both figures indicates 50  $\mu\text{m}$ .

In this study, we measured the signals produced by the cutoff levels of the protein biomarkers CA 242 and CEA that are relevant to the prognosis and diagnosis of pancreatic cancer. A relationship between the speed of repulsion of the PM functionalized with CA 242 and CEA antibodies was observed for both the frequency and the cutoff levels of each of these two antigens in the samples. In Figure 4, we show the drift velocity of repulsion due to DEP on PM functionalized with a CA 242 monoclonal antibodies at 0 U/mL, 10 U/mL, 20 U/mL, 40 U/mL in serum as a function of the frequency. The measurements were repeated six times to assess the accuracy of each measurement. Each 10  $\mu\text{L}$  droplet of the sample took 12 min to dry during the experiments. We plotted the standard deviation of the results using error bars as the indicator of the confidence levels of the calculated mean value of the drift velocity. In Figure 4, we observed no overlap between the confidence intervals of the DEP spectrum at 1.4 MHz and a partial overlap between the error bars at other frequencies. Therefore, the detection could be carried out using only six frequencies of measurement at 1.4 MHz. A further increase in the number of measurements would increase the accuracy of the concentration level. Further studies need to be carried out to investigate the sources of the variability in the measurements and how to minimize their impact on the signal acquired by the biosensor.

In Figure 5, we show the results of the detection of CEA in serum at 0 ng/mL, 5 ng/mL, 10 ng/mL, and 20 ng/mL concentration cutoff levels at a frequency range from 0.5 to 2 MHz. Since no overlap was observed in the confidence intervals measured at 1.7 MHz, that was the best frequency for determining the concentration level of CEA in serum. Unlike the DEP spectrum of PM functionalized for the detection of CA 242 shown in Figure 4, which did not have any clear feature standing above the confidence interval, the DEP spectrum of PM functionalized for the detection of CEA shown in Figure 5 had a maximum at 800 kHz and a broad minimum between 1.1 MHz and 2 MHz. That maximum at 800 kHz decreased with the increase in the concentration of CEA. A more detailed characterization of the spectral response would require the conduction of experiments with higher spectral resolution. The number of experiments per 10  $\mu\text{L}$  droplet of the sample was limited to 36 (6 different frequency measurements repeated 6 times) due to the evaporation of the droplet after 12 min. In both of these sets of experiments with CEA and with CA 242, the

DEP spectrum dropped with the increase in the number of cancer biomarkers bound to the functionalized PM.

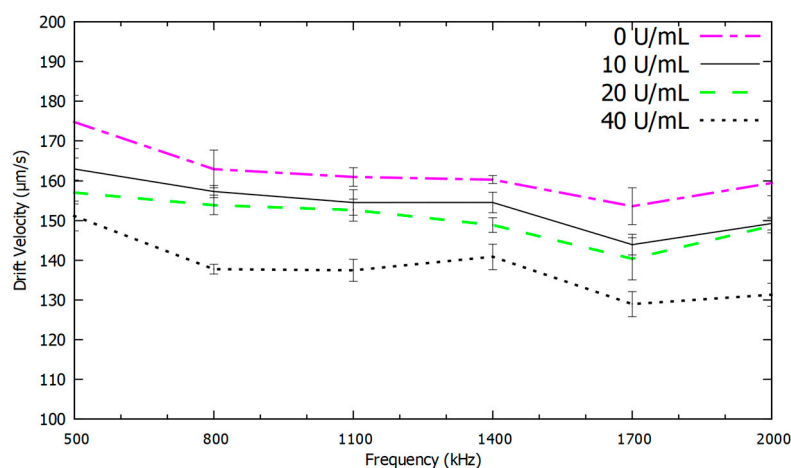


**Figure 4.** Negative DEP spectrum curves for cutoff levels of CA 242 for the detection of pancreatic cancer at 10 U/mL, 20 U/mL, 40 U/mL, and 0 U/mL. The 0 U/mL was a control sample without the native antigen of CA 242 in the sample to bind to CA 242-antibody functionalized PMs. The results shown in each frequency per curve are the mean of six measurements, and the error bars show their respective confidence intervals.

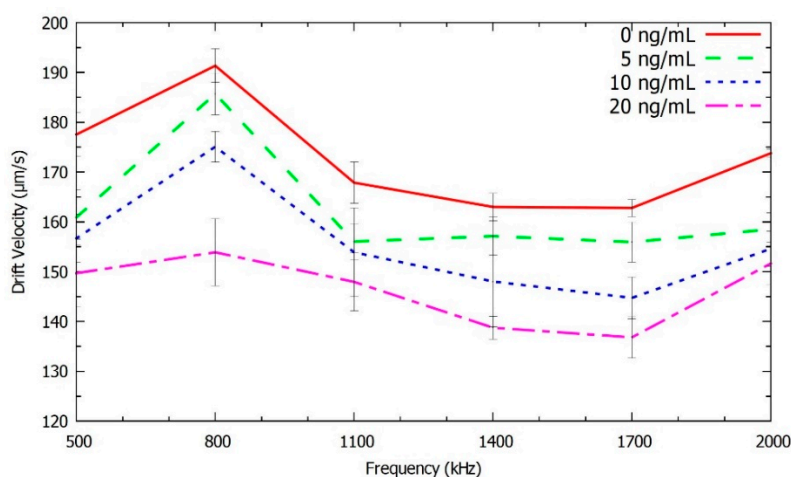


**Figure 5.** Negative DEP spectrum for the various concentration levels of CEA at 5 ng/mL, 10 ng/mL, 20 ng/mL, and 0 ng/mL. The 0 ng/mL was a control sample without the native antigen of CEA in the sample to bind to CEA antibody functionalized PMs. The results shown in each frequency per curve are the mean of six measurements, and the error bars show their respective confidence intervals.

The transduction mechanism of this biosensor is due to the change in the charge distribution near the surface of the PM, which was functionalized with antibodies to the target cancer biomarkers in the sample, since that determines the DEP force. When the serum sample has a higher concentration level of the cancer biomarker, a larger number of binding sites on the PM functionalized with antibodies are bound to the antigens. That increase in the molecule binding affects the charge distribution near the surface of the PM in a manner that is frequency-dependent. In both assays, the increase in the number of antigens bound to the antibody binding sites decreased the DEP force. That was due to differences in how charges distribute around the PM-bound antibodies that are partially bound to antigens. Even though the particular dependence of the DEP force acting on PM bound to biomolecules as a function of the frequency is not well understood [39], that phenomenon can be exploited in the development of biosensors through experimental

investigations. A study of how the DEP force on functionalized PM depends on the particular molecular structures of the antibodies and the antigens bound to the antibodies of CEA and CA 242 on PM surfaces is beyond the scope of this study.

#### 4. Conclusions

We demonstrated that the negative DEP spectroscopy was an effective transduction mechanism for the detection and analysis of the pancreatic cancer biomarkers CA 242 and CEA in serum. This technique was rapid and it did not require the use of fluorescent labels. Therefore, it did not require the washing of unbound fluorescent molecules in the sample preparation procedure, and it did not require careful calibration of the light source and the photodetector sensitivity. The spectroscopic signature of the biomarkers obtained with this technique did not depend on the light intensity or the sensitivity of the microscope camera. These results were obtained using an electrode array that has a well-defined gradient of the electric field that enables repeatability of the experiments. Future studies need to be carried out to determine how the frequency-dependent DEP force on antibody-functionalized PM depends on the number of bound antigens and the molecular structures of both the antigen and the antibody molecules.

**Author Contributions:** Conceptualization, F.D.G. and I.T.L.J.; Formal analysis, F.D.G., S.G.G. and I.T.L.J.; Investigation, F.D.G. and I.T.L.J.; Methodology, F.D.G. and I.T.L.J.; Project administration, I.T.L.J.; Funding acquisition, I.T.L.J.; Validation, F.D.G., S.G.G. and I.T.L.J.; Writing—original draft, F.D.G.; Writing—review & editing, F.D.G., S.G.G. and I.T.L.J. All authors have read and agreed to the published version of the manuscript.

**Funding:** This research was funded by ND EPSCoR.

**Data Availability Statement:** Not applicable.

**Conflicts of Interest:** The authors declare no conflict of interest.

#### References

1. Siegel, R.L.; Miller, K.D.; Fuchs, H.E.; Jemal, A. Cancer Statistics, 2021. *CA Cancer J. Clin.* **2021**, *71*, 7–33. [[CrossRef](#)] [[PubMed](#)]
2. Hidalgo, M. Pancreatic Cancer: Overview. *Lancet* **2011**, *378*, 1605–1617.
3. Petrushenko, W.; Gundara, J.S.; De Reuver, P.R.; O’Grady, G.; Samra, J.S.; Mittal, A. Systematic review of peri-operative prognostic biomarkers in pancreatic ductal adenocarcinoma. *HPB* **2016**, *18*, 652–663. [[CrossRef](#)] [[PubMed](#)]
4. Bhat, K.; Wang, F.; Ma, Q.; Li, Q.; Mallik, S.; Hsieh, T.; Wu, E. Advances in Biomarker Research for Pancreatic Cancer. *Curr. Pharm. Des.* **2012**, *18*, 2439–2451. [[CrossRef](#)]
5. Kim, J.Y.; Hong, S.-M. Precursor Lesions of Pancreatic Cancer. *Oncol. Res. Treat.* **2018**, *41*, 603–610. [[CrossRef](#)]
6. Bhatt, A.N.; Mathur, R.; Farooque, A.; Verma, A.; Dwarakanath, B.S. Cancer biomarkers-current perspectives. *Indian J. Med. Res.* **2010**, *132*, 129–149.
7. Winter, J.M.; Yeo, C.J.; Brody, J.R. Diagnostic, prognostic, and predictive biomarkers in pancreatic cancer. *J. Surg. Oncol.* **2013**, *107*, 15–22. [[CrossRef](#)]
8. Gudagunti, F.D.; Velmanickam, L.; Nawarathna, D.; Lima, I.T. Nucleotide identification in DNA using dielectrophoresis spectroscopy. *Micromachines* **2020**, *11*, 39. [[CrossRef](#)]
9. Gudagunti, F.D.; Jayasooriya, V.; Afrose, S.; Nawarathna, D.; Lima, I.T. Biosensor for the characterization of gene expression in cells. *Chemosensors* **2019**, *7*, 60. [[CrossRef](#)]
10. Loosen, S.H.; Neumann, U.P.; Trautwein, C.; Roderburg, C.; Luedde, T. Current and future biomarkers for pancreatic adenocarcinoma. *Tumor Biol.* **2017**, *39*, 1–11. [[CrossRef](#)]
11. Kunovsky, L.; Tesarikova, P.; Kala, Z.; Kroupa, R.; Kysela, P.; Dolina, J.; Trna, J. The Use of Biomarkers in Early Diagnostics of Pancreatic Cancer. *Can. J. Gastroenterol. Hepatol.* **2018**, *2018*, 5389820. [[CrossRef](#)] [[PubMed](#)]
12. Bernard, V.; Kim, D.U.; San Lucas, F.A.; Castillo, J.; Allenson, K.; Mulu, F.C.; Stephens, B.M.; Huang, J.; Semaan, A.; Guerrero, P.A.; et al. Circulating Nucleic Acids Are Associated with Outcomes of Patients With Pancreatic Cancer. *Gastroenterology* **2019**, *156*, 108–118.e4. [[CrossRef](#)] [[PubMed](#)]
13. Cohen, J.D.; Javed, A.A.; Thoburn, C.; Wong, F.; Tie, J.; Gibbs, P.; Schmidt, C.M.; Yip-Schneider, M.T.; Allen, P.J.; Schattner, M.; et al. Combined circulating tumor DNA and protein biomarker-based liquid biopsy for the earlier detection of pancreatic cancers. *Proc. Natl. Acad. Sci. USA* **2017**, *114*, 10202–10207. [[CrossRef](#)] [[PubMed](#)]
14. Yuan, W.; Tang, W.; Xie, Y.; Wang, S.; Chen, Y.; Qi, J.; Qiao, Y.; Ma, J. New combined microRNA and protein plasmatic biomarker panel for pancreatic cancer. *Oncotarget* **2016**, *7*, 80033–80045. [[CrossRef](#)] [[PubMed](#)]

15. Madhavan, B.; Yue, S.; Galli, U.; Rana, S.; Gross, W.; Müller, M.; Giese, N.A.; Kalthoff, H.; Becker, T.; Büchler, M.W.; et al. Combined evaluation of a panel of protein and miRNA serum-exosome biomarkers for pancreatic cancer diagnosis increases sensitivity and specificity. *Int. J. Cancer* **2015**, *136*, 2616–2627. [[CrossRef](#)] [[PubMed](#)]
16. Xiao, D.; Ohlendorf, J.; Chen, Y.; Taylor, D.D.; Rai, S.N.; Waigel, S.; Zacharias, W.; Hao, H.; McMasters, K.M. Identifying mRNA, MicroRNA and Protein Profiles of Melanoma Exosomes. *PLoS ONE* **2012**, *7*, e46874. [[CrossRef](#)] [[PubMed](#)]
17. Sempere, L.F. Integrating contextual miRNA and protein signatures for diagnostic and treatment decisions in cancer. *Expert Rev. Mol. Diagn.* **2011**, *11*, 813–827. [[CrossRef](#)]
18. Liu, J.; Gao, J.; Du, Y.; Li, Z.; Ren, Y.; Gu, J.; Wang, X.; Gong, Y.; Wang, W.; Kong, X. Combination of plasma microRNAs with serum CA19-9 for early detection of pancreatic cancer. *Int. J. Cancer* **2012**, *131*, 683–691. [[CrossRef](#)]
19. Li, Y.; Qi, X.; Lei, C.; Yue, Q.; Zhang, S. Simultaneous SERS detection and imaging of two biomarkers on the cancer cell surface by self-assembly of branched DNA–gold nanoaggregates. *Chem. Commun.* **2014**, *50*, 9907–9909. [[CrossRef](#)]
20. Gudagunti, F.D.; Velmanickam, L.; Nawarathna, D.; Lima, I., Jr. Label-Free Biosensing Method for the Detection of a Pancreatic Cancer Biomarker Based on Dielectrophoresis Spectroscopy. *Chemosensors* **2018**, *6*, 33. [[CrossRef](#)]
21. Shukla, S.K.; Purohit, V.; Mehla, K.; Gunda, V.; Chaika, N.V.; Vernucci, E.; King, R.J.; Abrego, J.; Goode, G.D.; Dasgupta, A.; et al. MUC1 and HIF-1 $\alpha$  Signaling Crosstalk Induces Anabolic Glucose Metabolism to Impart Gemcitabine Resistance to Pancreatic Cancer. *Cancer Cell* **2017**, *32*, 71–87.e7. [[CrossRef](#)] [[PubMed](#)]
22. Gautam, S.K.; Kumar, S.; Dam, V.; Ghersi, D.; Jain, M.; Batra, S.K. MUCIN-4 (MUC4) is a novel tumor antigen in pancreatic cancer immunotherapy. *Semin. Immunol.* **2020**, *47*, 101391. [[CrossRef](#)] [[PubMed](#)]
23. Van Manen, L.; Groen, J.V.; Putter, H.; Vahrmeijer, A.L.; Swijnenburg, R.-J.; Bonsing, B.A.; Mieog, J.S.D. Elevated CEA and CA19-9 serum levels independently predict advanced pancreatic cancer at diagnosis. *Biomarkers* **2020**, *25*, 186–193. [[CrossRef](#)] [[PubMed](#)]
24. Huang, H. Matrix Metalloproteinase-9 (MMP-9) as a Cancer Biomarker and MMP-9 Biosensors: Recent Advances. *Sensors* **2018**, *18*, 3249. [[CrossRef](#)] [[PubMed](#)]
25. Hasan, S.; Jacob, R.; Manne, U.; Paluri, R. Advances in pancreatic cancer biomarkers. *Oncol. Rev.* **2019**, *13*, 410. [[CrossRef](#)] [[PubMed](#)]
26. Lei, X.F.; Jia, S.Z.; Ye, J.; Qiao, Y.L.; Zhao, G.M.; Li, X.H.; Chang, H. Application values of detection of serum CA199, CA242 and CA50 in the diagnosis of pancreatic cancer. *J. Biol. Regul. Homeost. Agents* **2017**, *31*, 383–388. [[PubMed](#)]
27. Feng, L.; Gu, S.; Wang, P.; Chen, H.; Chen, Z.; Meng, Z.; Liu, L. Pretreatment values of bilirubin and albumin are not prognostic predictors in patients with advanced pancreatic cancer. *Cancer Med.* **2018**, *7*, 5943–5951. [[CrossRef](#)]
28. Jelski, W.; Mroczko, B. Biochemical diagnostics of pancreatic cancer—Present and future. *Clin. Chim. Acta* **2019**, *498*, 47–51. [[CrossRef](#)]
29. Ansari, D.; Torén, W.; Zhou, Q.; Hu, D.; Andersson, R. Proteomic and genomic profiling of pancreatic cancer. *Cell Biol. Toxicol.* **2019**, *35*, 333–343. [[CrossRef](#)]
30. Zhang, Y.; Yang, J.; Li, H.; Wu, Y.; Zhang, H.; Chen, W. Tumor markers CA19-9, CA242 and CEA in the diagnosis of pancreatic cancer: A meta-analysis. *Int. J. Clin. Exp. Med.* **2015**, *8*, 11683–11691.
31. Lwin, T.M.; Murakami, T.; Miyake, K.; Yazaki, P.J.; Shivley, J.E.; Hoffman, R.M.; Bouvet, M. Tumor-Specific Labeling of Pancreatic Cancer Using a Humanized Anti-CEA Antibody Conjugated to a Near-Infrared Fluorophore. *Ann. Surg. Oncol.* **2018**, *25*, 1079–1085. [[CrossRef](#)] [[PubMed](#)]
32. Lwin, T.M.; Miyake, K.; Murakami, T.; DeLong, J.C.; Yazaki, P.J.; Shivley, J.E.; Clary, B.; Hoffman, R.M.; Bouvet, M. Fluorescent humanized anti-CEA antibody specifically labels metastatic pancreatic cancer in a patient-derived orthotopic xenograft (PDOX) mouse model. In Proceedings of the SPIE BiOS, San Francisco, CA, USA, 1 March 2018; Volume 10478.
33. Litman-Zawadzka, A.; Łukaszewicz-Zajac, M.; Gryko, M.; Kulczyńska-Przybik, A.; Mroczko, B. Serum chemokine CXCL8 as a better biomarker for diagnosis and prediction of pancreatic cancer than its specific receptor CXCR2, C-reactive protein, and classic tumor markers CA 19-9 and CEA. *Pol. Arch. Intern. Med.* **2018**, *128*, 524–531. [[CrossRef](#)] [[PubMed](#)]
34. Meng, Q.; Shi, S.; Liang, C.; Liang, D.; Xu, W.; Ji, S.; Zhang, B.; Ni, Q.; Xu, J.; Yu, X. Diagnostic and prognostic value of carcinoembryonic antigen in pancreatic cancer: A systematic review and meta-analysis. *OncoTargets Ther.* **2017**, *10*, 4591–4598. [[CrossRef](#)] [[PubMed](#)]
35. Kato, H.; Kishiwada, M.; Hayasaki, A.; Chipaila, J.; Maeda, K.; Noguchi, D.; Gyoten, K.; Fujii, T.; Iizawa, Y.; Tanemura, A.; et al. Role of Serum Carcinoma Embryonic Antigen (CEA) Level in Localized Pancreatic Adenocarcinoma: CEA Level Before Operation is a Significant Prognostic Indicator in Patients With Locally Advanced Pancreatic Cancer Treated With Neoadjuvant Therapy Followed by. *Ann. Surg.* **2020**. [[CrossRef](#)] [[PubMed](#)]
36. Xing, H.; Wang, J.; Wang, Y.; Tong, M.; Hu, H.; Huang, C.; Li, D. Diagnostic Value of CA 19-9 and Carcinoembryonic Antigen for Pancreatic Cancer: A Meta-Analysis. *Gastroenterol. Res. Pract.* **2018**, *2018*, 8704751. [[CrossRef](#)] [[PubMed](#)]
37. Pethig, R. Dielectrophoresis: Status of the theory, technology, and applications. *Biomicrofluidics* **2010**, *4*, 022811. [[CrossRef](#)] [[PubMed](#)]
38. Pethig, R.; Smith, S. *Introductory Bioelectronics for Engineers and Physical Scientists*; Willey: West Sussex, UK, 2013; ISBN 9781119970873.
39. Camacho-alanis, F.; Ros, A. HHS Public Access. *Bioanalysis* **2015**, *7*, 353–371. [[CrossRef](#)] [[PubMed](#)]